Science of the Total Environment 842 (2022) 156755

Contents lists available at ScienceDirect

Science of the Total Environment

journal homepage: www.elsevier.com/locate/scitotenv

Radioactive particles from a range of past nuclear events: Challenges posed by highly varied structure and composition

Mathew P. Johansen [a,*], David P. Child [a], Richard Collins [b], Megan Cook [c], Joel Davis [a], Michael A.C. Hotchkis [a], Daryl L. Howard [d], Nicholas Howell [a], Atsushi Ikeda-Ohno [e], Emma Young [a]

[a] Australian Nuclear Science and Technology Organisation (ANSTO), Locked Bag 2001, Kirrawee DC, NSW 2232, Australia
[b] University of New South Wales, Sydney, Australia
[c] International Atomic Energy Agency (IAEA), Environmental Laboratories, Monaco
[d] Australian Synchrotron, 800 Blackburn Road, Clayton, Victoria 3168, Australia
[e] Japan Atomic Energy Agency (JAEA), 2-4 Shirakata, Tokai-mura, Naka-gun, Ibaraki-ken 319-1195, Japan

HIGHLIGHTS

- Numerous and varied radioactive particles persist at all nuclear event sites studied.
- Si-,Ca- surface composition enable particle persistence, including in marine conditions.
- Our methods reveal a prevalence of interior fractures not previously recognised.
- Fractures often connect to particle surfaces and may facilitate radionuclide leaching.
- The study weapons-test particles were dominated by Pu (vs ^{137}Cs, ^{90}Sr).

GRAPHICAL ABSTRACT

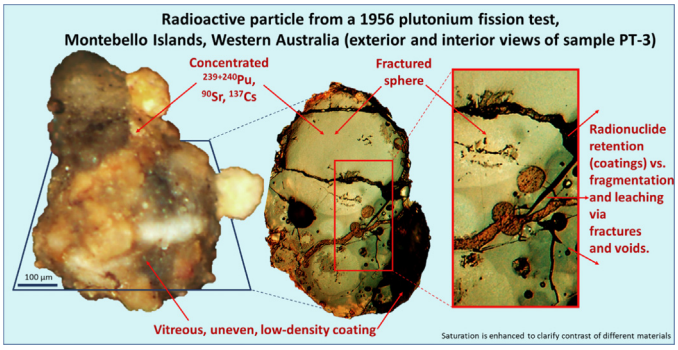

ARTICLE INFO

Editor: Filip M.G. Tack

Keywords:
Radiological and stable element composition
Nuclear weapons tests vs nuclear power accidents
Plutonium
Fallout
Debris
Hot particles

ABSTRACT

While they have appeared only recently in earth's history, radioactive particles from anthropogenic sources are widespread in global environments and present radiological harm potentials to living organisms. Exposure potentials vary greatly, however few studies examine a wide range of source and particle types. Here we compare a varied set of particles from past nuclear fission and non-fission sources in Australia of highly diverse magnitudes, release modes, and environments. The radiochemistry and microscopy methods revealed that numerous radioactive particles persist in soils 60+ years after their release events. Particles can be distinguished by their Ca/Fe and Si/Fe elemental ratios, which in this study range over orders of magnitude and reflect the materials available during their individual formation events. The particles with Si- and Ca-dominant compositions persisted in corrosive environments (e.g., marine). Internal fracturing is more prevalent than previously reported, and fracturing is greater in Ca-rich vs. Si-dominated matrices. The fractures often form connective pathways from the interior to exterior surfaces, increasing the potential to leach radionuclides into a host organism or the environment. The particles from nuclear testing have dominant $^{239+240}$Pu activity concentrations, relative to ^{90}Sr and ^{137}Cs, which increases long-term radiological hazard from alpha emissions if inhaled or ingested, and contrasts with particles from nuclear power accidents (e.g., Fukushima). Additional physical/chemical/radiological measurements are needed to fully understand long-term fate and hazard potentials.

* Corresponding author.
E-mail address: Mathew.johansen@ansto.gov.au (M.P. Johansen).

http://dx.doi.org/10.1016/j.scitotenv.2022.156755
Received 22 March 2022; Received in revised form 10 June 2022; Accepted 13 June 2022
Available online 16 June 2022

1. Introduction

Whether sourced from weapons explosions, nuclear power accidents or other activities, the ongoing behaviour of a radioactive particle is largely determined by the unique combination of source material, heat, pressure, and ancillary material brought together during its formation event (IAEA, 2011; Salbu et al., 2018). However, most studies on radioactive particles are limited to a single, or few, source events apparently because of the challenging nature of particle characterisation as well as political/geographical constraints in obtaining particles across multiple sites.

From 1952 to 1963 >600 distinct test events were conducted in Australia involving nuclear material (Burns et al., 1995; Long et al., 2021; MARTAC, 2003). The tests varied from small non-fission/partial fission tests to large fission detonations (12 tests), While the above-ground fission tests were fewer in number than at some other international sites (e.g., 23 at the Bikini Atoll), the series of tests in Australia represent a uniquely broad set of varied configurations (ship, tower, surface, air drop, balloon), range of energies (<1 kT to ~100 kT), use of varied source material (Pu and U fuel) and environments (arid desert to sub-tropical marine islands conditions).

Most of the tests were referred to as "safety trials" or "non-fission" tests in which a total of ~24 kg of plutonium (Pu) and >8000 kg of uranium (U) were subjected to fire, explosion, or other rapid releases of energy (MARTAC, 2003). High explosives were typically used and in a small number from this group, low-energy partial fission reactions were reported (MARTAC, 2003). While the explosive forces of the safety trials were less than the fission detonations, they produced larger contamination plumes with higher radionuclide levels in some areas (MARTAC, 2003).

In this study, we report on a set of radioactive particles representing a varied range of nuclear weapons test events. We prioritised particles from areas of greatest persisting radiological contamination. Most of these areas have had none, or scant, particle characterisation with one exception as detailed below. We use autoradiography, gamma and alpha spectroscopy, scanning electron microscopy (SEM) and X-ray fluorescence microscopy (XFM) to identify key structural features and quantify elemental and radiological composition. We test the applicability of these methods in highlighting particle features (e.g., elemental composition, fractures, and radiological content) that influence their persistence in the environment. Our main concern is to improve the understanding of particle contaminant forms in support of evaluating their ongoing environmental fate and potential impacts on the biosphere; a need that has been highlighted in recent review publications (e.g., IAEA, 2011; Salbu et al., 2018). This objective contrasts with the forensic focus of many previous publications although similar and complimentary analysis tools and processes are used (Belloni et al., 2011; Bellucci and Simonetti, 2012; Bonamici et al., 2016; Lewis et al., 2015; Weisz et al., 2017).

Radionuclide contamination occurs at sites around the world, and we provide a limited comparison with particles from the 2011 Fukushima and 1986 Chernobyl nuclear power accidents. Because the numerous source events in Australia (600+), and at international sites, far exceed the limited set of particles we evaluate here, the text also identifies knowledge gaps and requirements for future research to help manage ongoing radiological exposures.

2. Experimental

2.1. Sampling and sample preparation

Samples were gathered during 2011 and 2015 from locations at Maralinga, Emu and the Montebello Islands where nuclear tests took place from 1952 to 1963 as part of the British nuclear weapons development program (Child and Hotchkis, 2013; MARTAC, 2003). The tests caused fallout across Australia (Lal et al., 2017; Tims et al., 2013) with elevated concentrations over substantial areas near the test sites (Fig. 1). Soils (<4 cm) were gathered 250 to 500 m from most explosion/release sites (details in AT-1). However, at the Hurricane test site (ship test), the sample was gathered 1.6 km from the detonation location, on the closest nearby island, where monitoring indicated the detonation plume had deposited contamination. At the Vixen B site, Taranaki, the sample was gathered 2 km from the explosion location, just outside of the area remediated c. 2000 (Fig. 1). No recent remediations have since occurred and no archived samples were used; therefore, the study samples are representative of the major contamination areas that remain today. Because of the many tests conducted (>600), it was necessary to select a subset of representative particles based on the differing environments (marine-Montebello, arid-terrestrial at Maralinga and Emu), differing event energies (<1 kT to ~100 kT) and differing modes (tower vs ship tests). We identified six samples from dominant and lasting contamination plumes (Fig. 1).

Bulk soils were analysed by gamma spectroscopy (details in AT-2). Representative subsamples (5 g) of soil were thinly dispersed over a 20 × 40 cm plate in an aqueous solution (1:40 mass ratio of refined sugar ($C_{12}H_{22}O_{11}$) in deionised water). After drying at 60 °C, the solution solidified to a thin, transparent matrix that stabilised the sample for further processing. The immobilised samples were examined using photostimulated luminescence (PSL) autoradiography (described below), from which individual particles were identified and subsequently isolated and extracted with the aid of a microscope. The separated particles were rinsed in deionised water, dried, then affixed to polyimide or carbon tape and covered by <4 μm polyester film for analysis.

For brevity, when referring to the samples as a group, we use the generic terms "particles" although the largest object exceeds the nominal 2 mm diameter for particles proposed by Salbu et al. (2018). The same publication recommends the term "fragment" for larger nuclear debris, and here we use "fragment," or more specifically, "melt-glass fragment" when referring to the larger sample individually. Including a melt-glass fragment in the subset here aligns with the study objective of describing contamination at the study sites, many of which include melt-glass.

2.2. Particle samples and their source information

Understanding the ongoing exposure potentials that radioactive particles present to humans and the environment requires knowledge of their material properties. These in turn relate to the material available during their formation events. Previously, only one Australian site (Taranaki Safety Trials) was mentioned in a 2011 list of global sources of radioactive particles (IAEA, 2011) and this site has been the focus of past publications (Burns et al., 1995; Cook et al., 2021; Cooper et al., 1994; Ikeda-Ohno et al., 2016). Particles from this site display intricate physical and chemical composition consistent with formation via condensation and cooling of polymetallic melts (immiscible Fe–Al–Pu–U; and Pb ± Pu–U). Pu and U are present predominantly in micro- to nano-particulate forms, some with chemically reactive phases which are protected by their inclusion in metallic alloys (Cook et al., 2021) or encasing shells with lower radionuclide concentrations (Ikeda-Ohno et al., 2016). Evaluation of particles from the wide range of other Australian sources has only been reported indirectly (Johansen et al., 2019), or is now dated (e.g., ARL, 1990).

For each study particle, historical information on source material is summarised here from: (ARL, 1986, 1990; Burns et al., 1995; Long et al., 2021; MARTAC, 2003). The acronyms used are: **PSh**-Particle from Ship test, **PT**-Particle from a Tower test, **MGT**-Melt Glass from Tower test and **PST**-Particle from a Safety Trials test (details in AT-1).

2.2.1. Samples from Pu-fission detonations

*2.2.1.1. Sample **PSh-1**, Hurricane test (25 kT), marine vessel, 3 October 1952, Montebello Islands.* Hurricane was the first nuclear fission detonation of the British weapons programme and first in the Southern Hemisphere. It tested the functionality of a Pu-core weapon design (Blue Danube) as well as blast/fallout effects on equipment, structures and biology. The detonation was at 2.7 m below the water line within the hull of the HMS Plym, anchored in 12 m of water within ~500 m of the nearest shoreline.

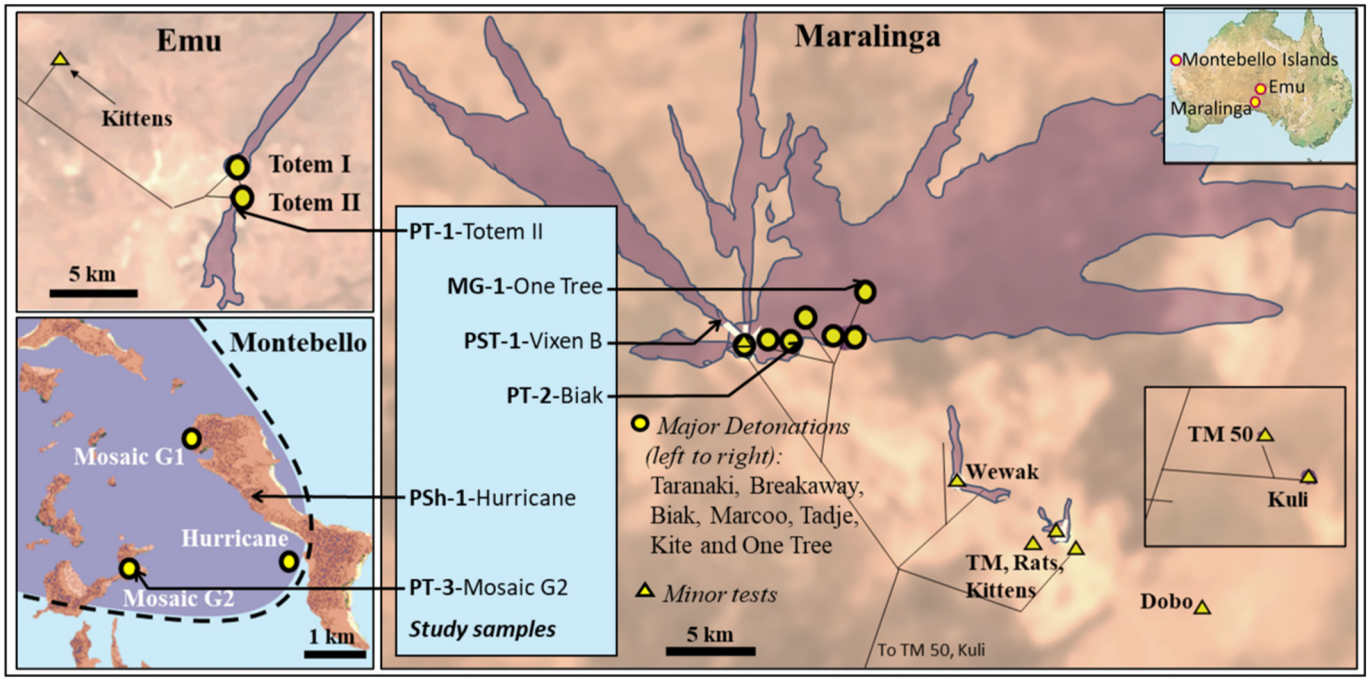

Fig. 1. Locations of samples relative to their sources and fallout deposition plumes. The contaminant contours at Emu and Maralinga are based on the most recent (1987) gamma survey showing areas of >1 kBq m^{-2} from ^{137}Cs, ^{238}U and ^{241}Am (MARTAC, 2003). Some areas near ground zero were remediated c. 2000 (e.g., Taranaki, Wewak, shown as white). Background images were processed from Aug 26, 2021 access of DigitalGlobe 2021, V.9.143.0.0, http://www.earth.google.com.

Included were high-explosive components, with Po, Be and U/Pu elements in the initiator, tamper and core, respectively. The Pu was mainly from the UK, supplemented by Pu from Canada. Support equipment included a range of metals in components of detonators, fuses, firing circuits, cabling and monitoring equipment. However, most material available for inclusion in the heat cloud was derived from the HMS Plym (Fe alloys dominant) as well as seawater and potentially marine sediments.

*2.2.1.2. Sample **PT-1**, Totem II test (7.1 kT), 31 m steel alloy tower, 26 October 1953, Emu (followed the Totem I test (9.1 kT), 4 October 1953).* The purpose of the Totem tests was to refine Pu weapon design, especially in evaluating varying amounts of ^{240}Pu in the core (~6 % relative to ^{239}Pu). The test weapons and support material were similar to that of the Hurricane test. The devices were detonated without bomb casings, and the steel-alloy support towers differed from the Al-alloy used in all other Australian tower tests. Site surface soils are derived mainly from the siliceous dunes and secondary calcrete units of the Great Victoria Desert (GVD), modified by iron-rich clay drainage pans and occasional silcrete rises. Major minerals of GVD sands are typically: SiO_2 (83–94 %), $CaCO_3$ (3–10 %), CaO (1–5 %), Al_2O_3 (1–2 %), Fe_2O_3 (0.7–1.3 %) and <0.5 % of MgO, TiO_2, K_2O, MnO, Na_2O, P_2O_5 and SO_3 (Sheard et al., 2006). Melt-glass was observed in recent site visits (since 2010) near ground zero at both Totem sites.

*2.2.1.3. Samples **PT-2** and **MGT-1**, Buffalo and Antler test series, 31 m Al-alloy towers, 1956–1957, Maralinga.* Sample MGT-1 is from the One Tree test (12.9 kT), 27 September 1956, which initiated the Buffalo series for testing smaller weapons designs (e.g., Red Beard) as well as biological and human response studies. Sample PT-2 is from the Biak test (5.6 kT), 25 September 1957; with a tower detonation similar to other Buffalo series (Breakaway (10.8 kT), 22 October 1956) and Antler series (Tadje (0.9 kT), 14 September 1957) detonations that tested aspects of thermonuclear designs. The Breakaway test included small quantities of light elements and the Tadje test included pellets of ^{60}Co to act as gamma detection tracers. Included were high-explosive components, with Po, U and Pu dominating in initiators, tampers and cores. Test equipment included a range of metals in the components of detonators, fuses, firing circuits, cabling and monitoring equipment. Surface soils are derived mainly from the surficial sands of the Great Victoria Desert (see above for Emu sites). Melt-glass was observed in recent visits (since 2010) at One Tree, Breakaway and Biak, but no significant amounts were observed at the low-yield Tadje site.

*2.2.1.4. Sample **PT-3**, Mosaic G2 test (~100 kT), 31 m Al-alloy tower, 16 June 1956, Montebello Islands.* The Mosaic test series (which also included the Mosaic G1 test (15 kT), 31 m Al-alloy tower, 16 May 1956) were conducted to evaluate the effects of the inclusion of light elements in precursor thermonuclear designs. Mosaic G2 was the largest test conducted in Australia and was initially reported to be consistent with a pre-test limit of 60 kT while later documents indicate the estimated yield to have been ~100 kT (UNSCEAR, 2000). Included were Pu cores, high-explosive components, and small quantities of thermonuclear material (lithium deuteride or lithium deuterotritide). Tampers were dominated by Pb (G1) and natural U (G2). Test equipment included a range of metals in the components of detonators, fuses, firing circuits, cabling and monitoring equipment. The Al-alloy support towers were 31 m in height. Surface soils are derived mainly from limestone as well as calcarenite and sandstone interbeds with substantial modification by windblown marine sediments (the test sites are within 200 m of the shoreline/marine waters). No melt-glass is mentioned in historical documents, and none was evident in recent site visits (since 2015) which is consistent with the low silicate levels in the surface soils.

Three additional fission detonations at Maralinga produced lesser contamination plumes and were therefore not chosen for representation in this study (Appendix A: Marcoo test (1.4 kT uranium-design), 4 October 1956; Kite air-drop test (2.9 kT), 11 October 1956; the Taranaki balloon test (26.6 kT), 9 October 1957).

2.2.2. Samples from non-fission and partial-fission testing

*2.2.2.1. Sample **PST-1**, Vixen B Safety Trials, 1959–1963, Maralinga.* The Pu-dominated Vixen tests investigated the responses of weapons assemblies to accidental forces (e.g., explosives, impact, fire). The Vixen A series (31 tests at Wewak) were mainly conducted to test the response to fires including the

dispersal of Pu, U and Be released in particulate forms. The Vixen B series (12 tests at Taranaki) tested designs on improving resistance to the effects of accidents during manufacture, storage or transport. The tests used simulated weapons assemblies subjected to high-explosive or fuel accelerant events (e.g., vertical jets). Limited fission reactions occurred in some Vixen B tests (which were intended to be of similar magnitude, or less, than the conventional explosives). The tests were conducted on steel-dominated platforms that prevented or limited soil influence/entrainment during testing. The Vixen series used approximately 23 kg of Pu, 80 kg ^{238}U, 24 kg enriched U, and 26 kg Be. Ancillary material included steel, Pb, barytes bricks, concrete, natural or depleted U, enriched U and Be metal and polystyrene. Monitoring equipment cabling and instruments were reported to contain paraffin wax, steel, Al, Pb and plastics. Remediation occurred in the 1960s and 1990s which resulted in the removal of numerous fragments as well as surface soils over a large area (Long et al., 2021). The Vixen B test were only a small proportion of the total non-fission tests at Maralinga and Emu that produced radioactive particles (see Appendix A for details of other non-fission tests needing further study).

2.3. Analysis methods

Gamma spectroscopy was performed on soils and particles using an ORTEC High-Purity Germanium (HPGe) n-type reduced background detector (relative efficiency of 45 %) coupled to an ORTEC DSPEC Pro. MAESTRO software was used for peak resolution. For soils, an equivalent geometry, soil matrix, mixed gamma calibration source (15 × 55 mm, EZA SRS 94204) was used for energy and efficiency calibration across an energy range of 46.5–1836.1 keV. Count times were typically 24–72 h each to achieve adequate counting statistics.

Alpha spectrometry was conducted on bulk soils that were digested using a three-step digestion process: aqua regia reflux (solid:liquid ratio 1:20, 108 °C, 4 h); open hotplate digestion using hydrofluoric acid; and fusion digestion of residual solids. Sample digests were spiked with yield tracers and chemically processed as described in Harrison et al. (2011). $^{239+240}$Pu, ^{238}Pu and americium (^{241}Am) were measured by alpha spectrometry on a Canberra Alpha Analyst using Passivated Implanted Planar Silicon (PIPS®) detectors. Further method details are described in Harrison et al. (2011).

^{90}Sr quantification used the same digestion techniques as described for alpha spectrometry, and activity concentrations were quantified by Cherenkov counting on a Perkin-Elmer Tri-Carb 3100TR liquid scintillation counter. Instrumentation settings and count methodology are described in Harrison et al. (2011).

Photostimulated luminescence (PSL) autoradiography was used to distinguish the more active anthropogenic radioactive particles from the numerous surrounding natural grains. Samples were exposed to BAS-SR2040 imaging phosphor (IP) plates (Fuji Film, Japan), separated by a <4 μm polyester film, in a dark chamber for 3–6 days, depending on expected particle sizes and activity concentrations. The resulting stored luminescence was imaged on an FLA7000 (General Electric) variable mode laser scanner (IP settings). Data was output to tiff files which were down-sampled and convolved using FIJI (Image J) creating a 1:1 scale mask that could be printed onto standard laser printer transparency film. The mask was placed over the sample to indicate particle location. The pixel resolution of the images was fixed at 25 μm, although the point spread function (PSF) of the emissions varied with the isotopic composition and generally exceeded this. The autoradiography qualitatively indicated location and relative strength of the particles as emission sources. However, the technique used here probably underestimates particle densities as it captures a percentage, but not all, of the stochastically probable interactions with the phosphor.

Scanning electron microscopy-energy dispersive X-ray spectroscopy (SEM-EDS) was used to analyse the exterior surfaces of intact particles as well as the interior cross-sectional surfaces. Whole particles were embedded in epoxy resin, then slowly polished (using a diamond suspension to a 3 μm finish) until approximately 50 % of the particle was removed. The exposed surfaces were coated with approximately 50 Å of carbon under vacuum to prevent surface charging. The elemental composition and internal structure of the particle cross-sections were interrogated at discrete locations using the SEM-EDS coupled with electron backscattered imaging. Data were gathered using a Zeiss Ultra Plus system at an accelerating voltage of 15 kV with an attached Oxford Instruments X-Max 80 mm^2 silicon drift detector (SDD). Semi-quantitative elemental analysis was performed using Oxford AZtec software after quant optimisation using copper. The reported results are in weight percent (processing option "all elements analysed (Normalised)") and are relative to the elements Al, Ca, Cl, Fe, K, Mg, Mn, Na, O, P, S, Si and Ti. SEM data for the MGT-1 sample were not gathered; however, XFM data suggests composition similarity with PT-2 (Biak particle) as these were both tower tests conducted within 5 km and had similar soils.

X-ray fluorescence microscopy (XFM) was performed at the XFM beamline of the Australian Synchrotron under ring operating conditions of 3 GeV and 200 mA top-up mode (Howard et al., 2020). Samples were scanned at 18.070 keV using 0.4 × 0.4 um pixel size at 20 ms intervals. X-ray fluorescence spectra were fitted and the resulting images of elemental distribution were processed using GeoPIXE ™ (Version 7.4z; http://www.nmp.csiro.au/GeoPIXE.html) and FIJI Software. Elemental concentration maps were developed using the Dynamic Analysis matrix transform method as a function of incident beam energy. Further method details are described in (Howard et al., 2020).

3. Results and discussion

3.1. Persistence of particles at test sites

Numerous and readily identifiable radioactive particles persist at the study sites as indicated by PSL autoradiography images on bulk soils. For example, very small 5 g subsamples of soils from the Mosaic G2 (Fig. 2) and Vixen B sites (AF-1), respectively the largest and smallest explosive energies in this study, each contained 80–100 readily identifiable discrete particles. The numerous particles in the 5 g subsamples indicate that very large numbers of distinct particles persist in the contamination deposition areas which cumulatively extend over >100 km^2 across all sites. Although the particle densities are expected to decrease with distance from their release locations (Lukashenko et al., 2020), we document here that numerous particles occur near ground zero locations (e.g., Fig. 2) and at more

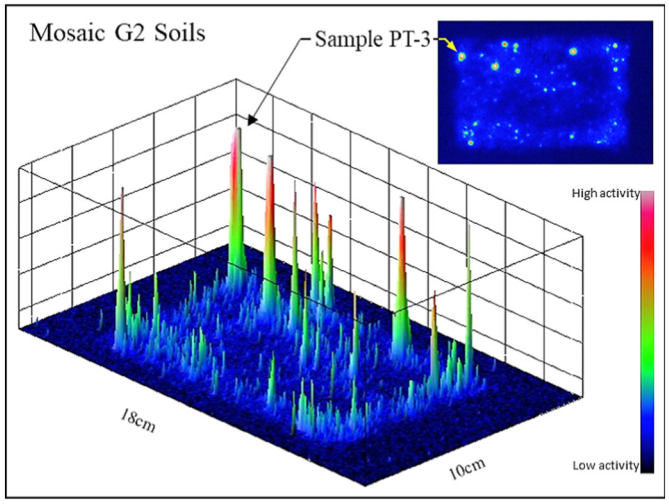

Fig. 2. Particle density image from PSL autoradiography of a typical 5 g soil subsample gathered from the Mosaic G2 site, Montebello Islands. Sample PT-3 is indicated. The measurement bar is relative emission intensity of primarily gamma and beta emissions (e.g., from ^{137}Cs, ^{90}Sr, and ^{241}Am). See AF-1 for additional sample images.

distant 1–2 km deposition areas (AF-1, Vixen B and Hurricane tests). Although decades of weathering have passed, most particles at the sites remain at or near the surface and are thus available for interaction with the biosphere (Johansen et al., 2016, 2014; Tims et al., 2013).

The sizes of the extracted particles/fragments in this study ranged over more than three orders of magnitude (Fig. 3, AT-1) with the smallest from the Vixen B safety trials, Maralinga, (PST-1, 57 μm longest axis) and the largest being the melt-glass fragment of the One Tree fission tower test (MGT-1, 11,400 μm). Considering the samples other than the melt-glass fragments, the maximum sizes observed on the autoradiography plates of aerially-formed particles were all <1000 μm. This observation is consistent with a conceptual model in which the size of aerially formed particles is mainly determined when coalescing droplets gain sufficient gravitational force to overcome the dissipating uplift forces; typically late in heat cloud progression (Bonamici et al., 2016; Weisz et al., 2017). This explanation implies that the size of aerially formed particles is relatively insensitive to explosive yield and in our samples there was little difference in the maximum particle sizes from highest- and lowest yield fission tests (Mosaic G2, ~100 kT vs Biak, ~6 kT).

Guided by the PSL autoradiography we isolated numerous particles and observed that greater proportions of finer particles are present. Log-normal tendency was apparent in the distribution of particle activities, and sizes,

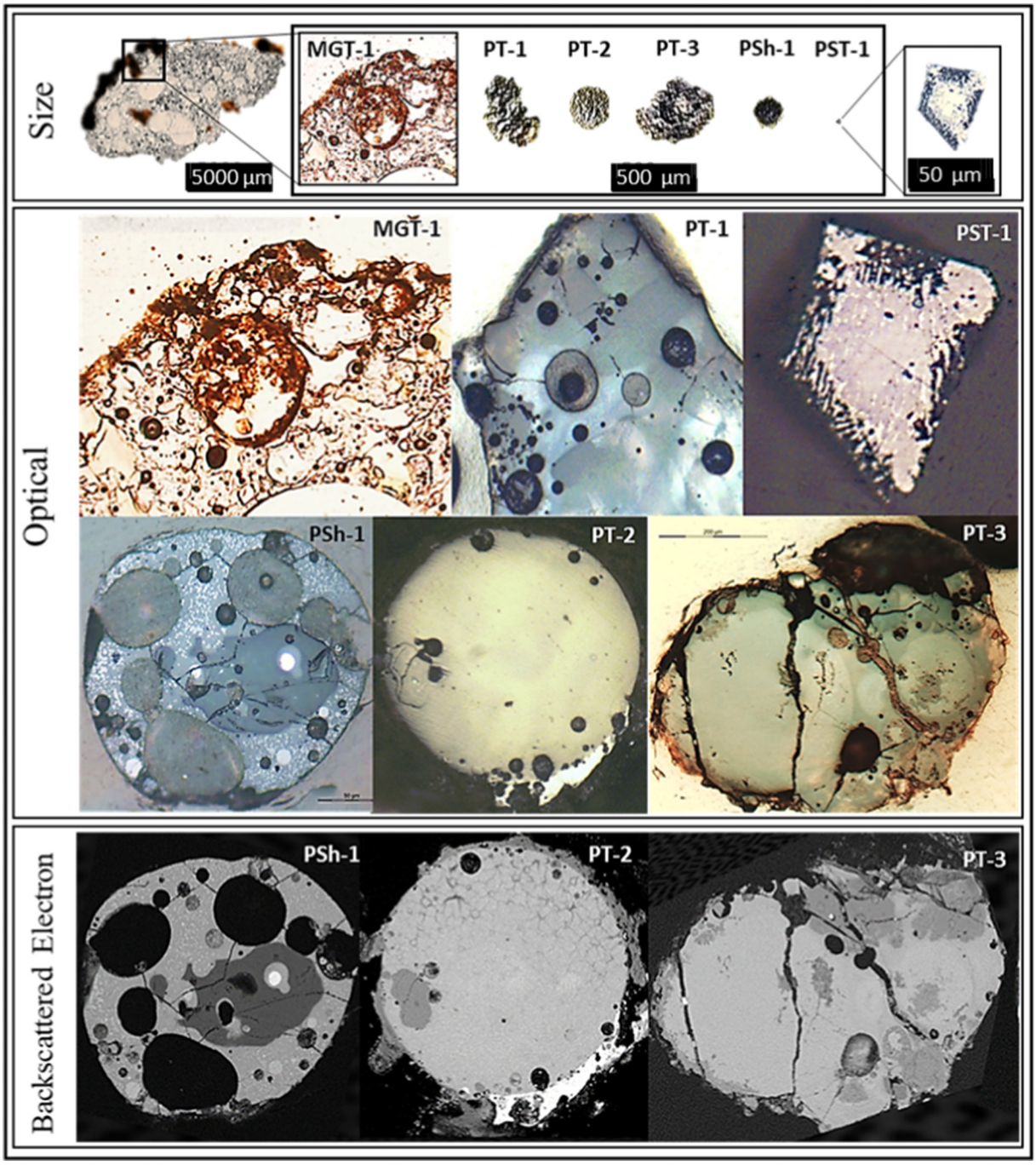

Fig. 3. Size comparison (top), optical views on polished cross-sections (middle) and SEM backscattered electron images (bottom). Shown are the MGT-1 melt-glass fragment (tower test One-Tree, Maralinga) and particles from tower tests PT-1 (Totem II, Emu), PT-2 (Biak, Maralinga) and PT-3 (Mosaic G2, Montebello Islands). Particle PSh-1 is from the ship-based test Hurricane, Montebello Islands, and PST-1 is from the Vixen B Safety Trials at Taranaki, Maralinga (see AT-1 for sample details). Images in the top "Size" panel are to scale, while images in the bottom two panels are of variable scale.

from all test types (terrestrial tower, marine ship, safety-trials surface platform). Similar distributions have been described at other nuclear event sites (IAEA, 2011; Jernström et al., 2006) with the proportion of the finer fraction increasing with distance (Lukashenko et al., 2020). In our study, distribution skewness appears to vary with release mode. While the Mosaic G2 and Hurricane tests were both conducted in the Montebello Island marine environment, the tower-based Mosaic G2 test readily subsumed site soils and created proportionally more of the larger-sized particles (in the 200–1000 μm size range). In contrast, the size distribution of the Hurricane ship test is skewed toward smaller particles formed mainly from Fe-alloy ship metals and sea salts (most were observed to be <10 μm, but were very active; AF-1).

The importance of the log-normal distribution tendency is that the more numerous finer particles are more easily mobilised, may travel further in earth systems (Pöllänen et al., 1997; Wendel et al., 2013) and can be more impactful to the health of humans and wildlife (Caffrey et al., 2017; Lind et al., 2020). For mammals, particles <5 μm may lodge deeper in the lungs and, if not cleared, present an ongoing risk from direct emissions as well as the leaching of radionuclides into the bloodstream and transport to other parts of the body (Durbin, 1975; ICRP, 1986).

3.2. Surface coatings, fractures and voids

The studied particles have varied and distinct structural features including surface coatings, fractures and voids, which may influence leaching, surface reactivity, and dose potentials of particles in the environment. Examples of surface coatings include PT-3, which appears glassy and lustrous when viewed as a whole particle (graphical abstract) which, when the interior was exposed, was revealed as an uneven coating of lower-density material (darker material in the Optical panel, Fig. 3). This glassy coating appears to be a late-stage condensate that was still molten when several small grains adhered to its exterior (graphical abstract image).

Sample PT-3 was gathered from island soils near the Mosaic G2 site and has much less pitting/weathering than that of a comparable particle retrieved from the nearby marine sediments (AF-2). Both particles originated from the same test and have nearly identical composition (AF-2 insets). The greater pitting in the particle retrieved from marine-sediments implies accelerated breakdown and eventual dissolution in marine waters. Although degraded, the coating is, overall, still intact which may explain the persistence of numerous such particles that remain in the corrosive marine conditions 60 years after the Mosaic G2 test (AF-1). The persistence of these particles has implications for ecological persistence of particles with similar composition and environmental distribution such as the glassy ^{137}Cs-rich particles dispersed in the marine environment from the Fukushima accident (Miura et al., 2021).

In contrast, readily-identifiable particles have not yet been found in marine samples from the nearby Hurricane ship test (Fig. 1), even though the sediments at that site contain elevated activity concentrations of ^{137}Cs, ^{90}Sr, ^{238,239,240}Pu, and ^{241}Am (based on seven sediment samples reported in Johansen et al., 2019). The close-in fallout from the Hurricane detonation was intense (Johansen et al., 2020) and some of this fallout was particulate, as demonstrated by PSh-1, which was retrieved from nearby island soils. The PSh-1 composition matches that of mainly ship metals and it has no substantive vitreous coating (Table 1, Fig. 3). This suggests that the numerous Hurricane ship-test particles that fell into marine waters in 1952 were mainly comprised of unprotected Fe-dominated material and have since been readily oxidised and dissipated. However, the lack of particles derived from the Hurricane test could also be due to burial by sedimentation processes rather than disintegration and more investigation of sediment depth profiles near the shallow sea detonation site is needed.

In addition to providing a protective surface, we document here that the surface coating of PT-3 appears to have prevented fragmentation during particle formation. The interior of PT-3 contains several captured spheres (Fig. 3, Optical) that have high symmetry as well as compositions that are relatively homogeneous. During particle formation, two complete fractures occurred in the largest sphere (Fig. 3, Optical, left) and another fracture developed around the surface of the 2nd largest sphere (Fig. 3, Optical, mid-right). While the fractures extend entirely through the material of the inner particle, they are capped by the coating material indicating the fractures occurred after conglomeration and after the coating was well established. Of these fractures, the left two are partially filled from the ends with the coating material, while the rightmost (largest) fracture had been fully filled. While the fractures were substantial, and displacement occurred, complete separation appears to have been prevented by the pliable coating. The fractures in PT-3 are the largest of the studied samples and this is consistent with its relatively high Ca content (Table 1). Higher Ca-content matrices are typically more susceptible to fracturing (Chen et al., 2021; Li et al., 2020).

While the large fractures of PT-3 are the most visible of the samples (Fig. 3), all particles had fractures on close inspection. These fractures varied in size, linearity and connectivity and some aspects could be related to their respective sources. In PSh-1, the fractures tend to be linear in the Fe-dominated areas, consistent with ductile-to-brittle cooling of a Fe-alloy cubic crystal matrix (Pineau et al., 2016). However, in the same particle, the fractures are smaller and more erratic in the large inclusion of lower-Fe and higher Si-oxide material (dark grey area, centre-right; Fig. 3, SEM panel) that we interpret to include sea sediments drawn from below the ship.

The PSh-1 fractures form a network, connecting most voids (black ellipsoidal shapes in Fig. 3 SEM-BSE panel). The voids are numerous, and their combined surface area approximates that of the outer surface area of this particle. This network of voids is connected to the outer particle surface by fractures in at least 16 locations in the exposed cross-section (which suggests many more void-to-surface connections around the sphere). Similar connectivity occurs in PT-2 which has networks of fine fractures, or potentially veins of lighter density material, some of which are connected to the particle surface (Fig. 3, SEM-BSE panel).

Radionuclides of concern are often concentrated inside the particle (Cook et al., 2021; IAEA, 2011; Ikeda-Ohno et al., 2016) and often it is assumed they may be insulated from the environment by surface coatings. We document here connectivity of fractures from the interior to the particle surface that may facilitate mobilisation of radionuclides into the environment via leaching following moisture uptake from precipitation, condensation, or inundation. However, the role of such fractures in radionuclide leaching is poorly understood, in part because the fractures remain hidden when using most characterisation methods that assess whole particles. In this study, the details of fractures and voids were made clear only after exposing the interior cross-sections. Other methods may reveal more

Table 1
Approximate weight percent of key elements as measured by SEM-EDS on exposed particle interiors [mean and (standard deviation)].

	PT-1	PT-2		PT-3	PSh-1	PST-1	Background	
		Interior	Coating				Maral-inga	Monte-bello
Ca	1 (0.2)	18 (10)	3 (2)	31 (14)	1 (0.5)	0.1 (0.2)	0.7 (0.4)	35 (8)
Fe	18 (10)	4 (2)	22 (11)	5 (4)	53 (22)	12 (11)	9 (7)	2 (0.3)
Si	29 (13)	30 (11)	7 (3)	18 (9)	7 (7)	2 (3)	33 (11)	2 (0.8)
Al	8 (3)	7 (3)	2 (0.6)	7 (3)	1 (0.5)	28 (25)	7 (0.4)	1 (0.3)
O	38 (6)	40 (5)	32 (3)	35 (5)	20 (10)	7 (9)	43 (7)	58 (7)
Highest other	Zr	Mg	Ti	Mg	Cu	Pu	K	Mg
	17 (24)	1 (0.7)	34 (10)	2 (3)	15 (25)	30 (3)	1 (0.4)	0.8 (0.4)

about fractures including the Focused Ion Beam Scanning Electron Microscopy (FIB-SEM) used in (Cook et al., 2021) and the Nano-CT methods in Salbu and Lind (2020) which would ideally be coupled with particle leaching experiments.

3.3. Variation of Ca, Fe, and Si composition

Given the observations on coatings and fractures suggest that Ca, Fe, and Si are important to the structural integrity and leaching potentials of the radioactive particles, we evaluated internal Ca/Fe and Si/Fe ratios of the samples. We used Fe content as a comparison basis due to its prevalence in study particles, its importance for understanding particle composition patterns (Bonamici et al., 2016; Weisz et al., 2017) and its relevance to potential radiological interactions (e.g., Pu is known to follow Fe metabolic pathways when entering the bodies of mammals (Durbin, 1975)).

Using the Ca/Fe and Si/Fe ratios, the data groupings were distinct (Fig. 4; $p < .01$. Kruskal-Wallis Test for both Ca/Fe and Si/Fe). The Ca/Fe variation was large (>10^4 across mean values) and exceeded the Si/Fe variation (>10^2). The ratio differences between individual particles are consistent with information on the source and ancillary material that was available during their formation. For example, the PSh-1 and PT-3 particles both came from the Montebello Islands (collected within 3.2 km of each other), yet their Ca/Fe ratio data ranges over nearly 10^4 which reflects the lack of soils for the Hurricane ship test vs the availability of Ca-rich soils for the Mosaic G2 tower test (Ca proportions of PT-3 match background soils: Table 1). The highest Si/Fe was in the interior of PT-2 (Biak) which had an elevated Si content that matched well with non-radioactive sand grains from the host Maralinga site (30 % and 33 % Si, respectively, Table 1). However, the ratios of PT-2s exterior surface coating are distinct (darker and lighter areas respectively in the SEM panel, Fig. 3). The denser section has much higher proportions of Fe and Ti (Table 1) suggesting it was derived from the Fe-rich soil layer below the surficial Great Victoria Desert sands at Maralinga.

The particles with low Ca/Fe ratios reflect higher Fe content as in PSh-1 (>50 % as measured by SEM-EDS and XFM) (Table 1, AT-3). Large amounts of Fe became available for incorporation into PSh-1 during the Hurricane test as the intense pressure and heat disintegrated much of the HMS Plym ship. The PST-1 particle from the safety trials test site also has elevated Fe, consistent with the steel-dominated support used in the Vixen B test beds (MARTAC, 2003) along with an unknown amount in the original test material. The XFM data on PST-1 indicate substantial amounts of Fe within the interior (Fig. 5) which is not, however, highly mixed as suggested by SEM-EDS data on the exposed cross-section in which the Fe was negatively correlated ($r = -0.72$) with the other major metal Pu.

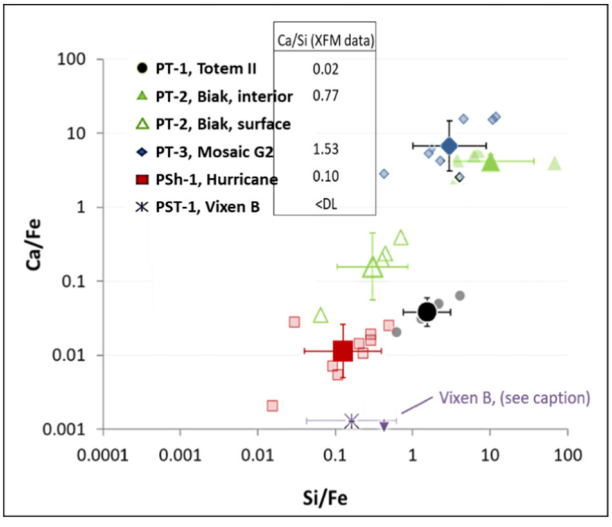

Fig. 4. Si/Fe and Ca/Fe ratios from SEM-EDS compositional data on the exposed particle cross-sections. Large symbols are geometric means (GMSD whiskers). The Si/Fe geometric mean and GMSD range of the Vixen B sample are graphed at the approximate Ca/Fe upper bound based on the single available measurement above DL (others were below DL, AT-4). The inset shows whole-particle Ca/Si ratios based on XFM data (AT-3).

The Fe in PT-1 is heterogeneous, with no apparent formation layering (Fig. 5). From this same Totem II test, we compare another particle that has similar heterogeneous interior Fe, but also has a clearly defined and relatively homogeneous Fe-rich surface layer (comparison particle, inset Fig. 5). This layer could have been formed by the fractionation-condensation effect that has been conceptualised in many papers (summarised by Bonamici et al., 2016; IAEA, 2011; Weisz et al., 2017). We make this comparison because such clear refractory fractionation, much discussed in previous papers, is lacking from PT-1 from the same test, and in the majority of our study particles as well.

Overall, the results here demonstrate the capability of using Ca-Fe-Si ratio data to distinguish particles formed from different event types and locations. The fission test particles with relatively high Ca/Fe and low Si/Fe ratios also had the largest fractures. The particles with elevated Fe-content suggest increased susceptibility of interior radionuclides to leaching and dissolution over time although the in-particle distribution of Fe is highly variable.

3.4. Variation in radiological content

In this analysis, we compare ^{90}Sr, ^{137}Cs and $^{239+240}$Pu because these often emerge as key radionuclides of concern after nuclear incidents due to the dose potentials of their energetic emissions, their abundance in nuclear waste forms and their persistence in the environment (Eriksson et al., 2008; IAEA, 2011; Lind et al., 2007; Lukashenko et al., 2020; Sancho and García-Tenorio, 2019; Whicker and Schultz, 1982). The studied particles had variable activity concentrations (AT-5, 6), with some being highly elevated (the $^{239+240}$Pu of MGT-1 and PST-1 are 2×10^5 and 3×10^8 Bq/kg respectively).

In all the studied particles, the $^{239+240}$Pu activity concentrations were dominant ranging from 66 % to 99.9 % of activity concentrations relative to ^{90}Sr and ^{137}Cs (Fig. 6, AT-5, 6). This mainly reflects the Pu composition of the source material (Pu-weapons tests) and the longer half-lives of Pu isotopes (^{239}Pu = 24,110 y vs. ^{90}Sr = 29 y, ^{137}Cs = 30 y). In addition, during fission tests, the precursors to ^{90}Sr and ^{137}Cs include halogens and noble gases that may be carried greater distances prior to decay and incorporation into particles.

The sample with the greatest Pu content (PST-1) is from a non-fission Vixen B tests, Maralinga, and has some similarity to other Pu-rich particles previously documented from this site (Burns et al., 1995; Cook et al., 2021; Ikeda-Ohno et al., 2016) and at other nuclear weapons accident sites (Eriksson et al., 2008; IAEA, 2011; Lind et al., 2007; Lukashenko et al., 2020; Sancho and García-Tenorio, 2019; Whicker and Schultz, 1982). However, the PST-1 particle differs in that it has largely retained sharply defined edges (Fig. 3) indicating little molten reworking following fragmentation. This contrasts with the molten-reworked particles from the same site studied previously (Burns et al., 1995; Cook et al., 2021; Ikeda-Ohno et al., 2016). These are mainly fragments of polymetallic melts (immiscible Fe–Al–Pu–U; and Pb ± Pu–U) that were formed from safety trials source material and modified during the high-explosive/jet fuel tests. In one such particle, the Pu(IV) oxyhydroxide-dominant core was surrounded by an external layer containing Ca, Fe, and U (Ikeda-Ohno et al., 2016). Cook et al. (2021) demonstrated that the interior Pu in safety trials particles can occur as discrete crystalline grains of highly concentrated (Pu, U)$O_{2\pm x}$ that in many cases align with structural edges and interfaces within the particles. Unresolved is whether these Pu concentrations are always limited to particle interiors or whether they may also occur on particle exteriors and along fragment edges where

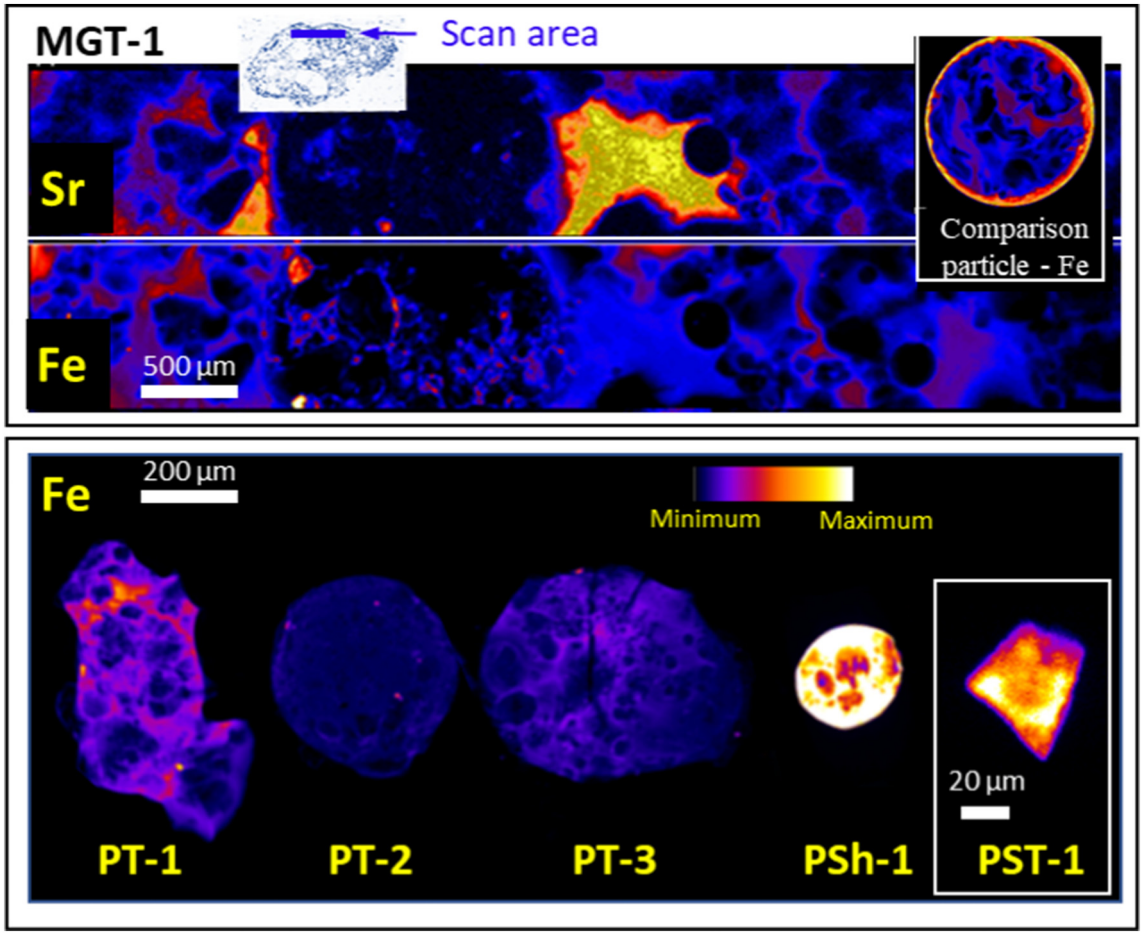

Fig. 5. Relative Fe composition as estimated by XFM on study samples. Fe and Sr are shown within a specific scan area of the larger MGT-1 sample (see AT-3 for XFM data details). The comparison image (upper right inset) is from an Emu, Totem II particle evaluated previously (COMET, 2017).

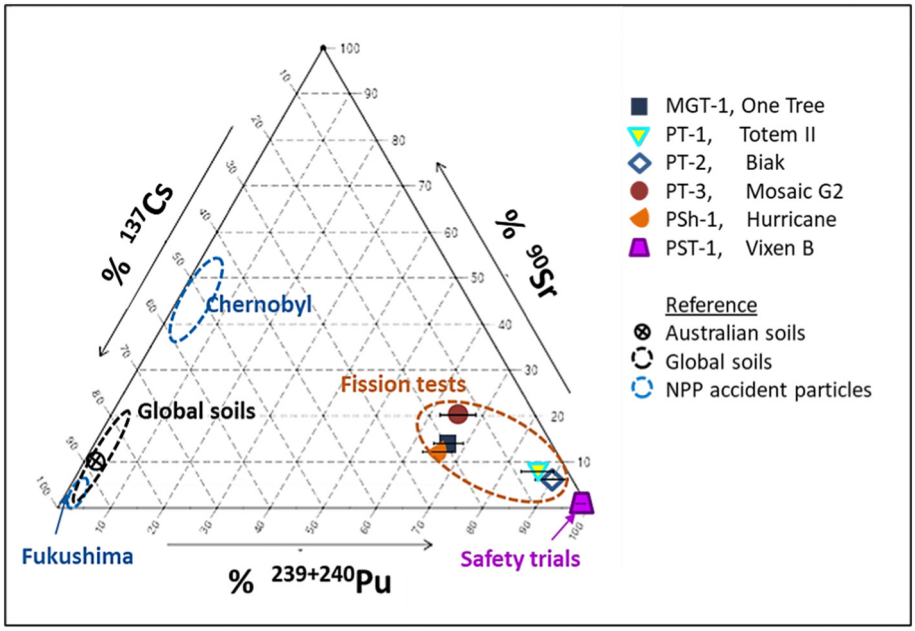

Fig. 6. Estimated relative percentages of ^{137}Cs, ^{90}Sr and $^{239+240}$Pu activities in the study samples. Horizontal whiskers are 1σ counting uncertainties on $^{239+240}$Pu in the individual particles (or inferred $^{239+240}$Pu from ^{241}Am). Data are on a Nov 2015 basis. Fukushima and Chernobyl data from Igarashi et al. (2019) and Papp et al. (1997). Global and Australian soils data from Hancock et al. (2011), Kim et al. (1998), Smith et al. (2016) and this study.

they could increase organism dose (Caffrey et al., 2017; Caffrey et al., 2015).

^{137}Cs, ^{90}Sr and Pu have also been documented in particles released from nuclear power plant (NPP) accidents, but with Pu at much lower proportions than ^{137}Cs and ^{90}Sr (Igarashi et al., 2019; Kurihara et al., 2020; Muramatsu et al., 2000). NPP fuel is predominantly U with fractional amounts of Pu (Konzen, 2016; Kuriny et al., 1993). NPP accident release temperatures are also low relative to nuclear detonation tests such as the relatively low-heat hydrogen explosions at Fukushima that were sufficient to volatilise compounds containing ^{137}Cs, but not the more refractory ^{90}Sr even though both were abundant in the NPP source material (^{90}Sr/^{137}Cs ratios ranged from 0.001 to 0.004 (Nakamura et al., 2018) vs a mean of 1.1 for this study). Similarly, at Fukushima, Pu was released in relatively low amounts (Johansen et al., 2021; Kurihara et al., 2020; Zheng et al., 2013). The reactor core fire of Chernobyl also had low temperatures relative to the study detonation tests, but was of sufficient heat, and open to the atmosphere, allowing for dispersal of particles with both ^{137}Cs and ^{90}Sr (Fig. 6, (Papp et al., 1997)) as well as Pu in higher amounts of Pu than Fukushima (Burakov et al., 2003; Kashparov et al., 2019; Muramatsu et al., 2000).

The main point of the ^{90}Sr, ^{137}Cs and ^{239,240}Pu comparison is that most of the weapons-test particles studied here have much greater amounts of long-lived Pu isotopes than the NPP particles. The ^{137}Cs activities can be similar depending on size (~1 Bq; this study and (Abe et al., 2021; Satou et al., 2016)). However, the weapons-test particles studied here have much greater ^{90}Sr (than Fukushima) and Pu (than Fukushima and Chernobyl); (1–219 Bq $^{239+240}$Pu for study particles vs 4–92 $\times$ 10^{-3} Bq (Chernobyl) and 1-7 $\times$ 10^{-5} (Fukushima)) (Igarashi et al., 2019). The weapons-test particles therefore have increased beta and alpha dose potential when inhaled or ingested and the alpha emissions from Pu will remain for thousands of years vs decades for the gamma and beta emissions from ^{137}Cs and ^{90}Sr. However, dose rates from specific particles may vary greatly depending on not only radionuclide composition, but also particle sizes, exposure routes, exposure time, and leaching potentials.

Some close-in particles from Fukushima and Chernobyl are relatively large (up to ~400 μm) (Martin et al., 2020; Morooka et al., 2021). Although these larger NPP particles have low Pu content (Igarashi et al., 2019; Kurihara et al., 2020), they would have external (skin) exposure rates from gamma or beta radiation similar to the larger weapons-test particles (e.g., MGT-1 has dense beta and gamma emissions clustered at its edge; inset Fig. 3 and AF-3). Some larger NPP particles (e.g., Martin et al., 2020; Morooka et al., 2021) have greater amounts of Ca and Fe and more complex structures vs the smaller NPP particles studied by Yamaguchi et al. (2016) which have relatively high SiO_2 (69 wt%) with lower Fe and Ca. A more detailed comparison of these structural and compositional differences is needed to determine their relative radionuclide leaching/dissolution potentials and potential dose impacts.

4. Requirements for future research

Comparing the varied samples of this study has revealed knowledge gaps relevant to radioactive particles acting as ongoing sources of human and environmental exposure. New data or applications that we have identified include:

- Better quantification of particle size distribution with emphasis on the more impactful (and more difficult to characterize) sub-μm sizes.
- Improved understanding of inter- and intra-source variation in particle composition and structure.
- Further evaluation of Ca, Si and Fe ratio data as predictors for fragmentation, weathering and leaching.
- Further evaluation on the Si- and Ca-composition of the outer surfaces of particles and how these relate to persistence/dissolution in corrosive environments (e.g., persistence of tower-based Mosaic G2 particles in marine sediments vs lack of ship-based Hurricane in marine sediments).
- A systematic method is needed for quantifying the degree of fracturing in radioactive particles that provides information on the role of fractures in persistence/disintegration rates as well as leaching potentials.
- The leaching and disintegration differences among particles from different sources have not been adequately studied. New particle-leaching data are needed including the role of fractures in leaching radionuclides and a comparison of leaching rates over a broad set of particle types.
- Application of microscopy to further evaluate instances when Pu may concentrate on exterior surfaces important for biosphere interactions.
- Improved source-assignment using ratios of key isotopes of Pu (e.g., ^{239}Pu, ^{240}Pu, ^{241}Pu), U (^{235}U, ^{236}U, ^{238}U), neutron activation (e.g., ^{152}Eu) and fission products (e.g., ^{137}Cs). The proximity of some tests (Fig. 1) complicates the source-assignment of some particles. In addition, while such isotopic analyses have been successfully applied to bulk soils and biological samples (Child and Hotchkis, 2013; Hotchkis et al., 2019; Tims et al., 2013), such data are scarce for radioactive particles.

5. Conclusions

Radioactive particles are persistent and numerous in soil samples from fission detonation and safety trials test sites many decades after their formation events. The concentrations of radionuclides in these particles are substantial and may cause direct external and internal exposure to humans and non-human biota. However, exposure/dispersal potentials can vary widely among particles and in this study we describe the following key contributing attributes:

- Larger proportions of finer particles persist (lognormal size distributions are typical). These are more easily mobilized/transported and can potentially be more impactful to the health of humans and wildlife;
- Si- and Ca-rich surface layers are present on some particles and provide apparent protection from dissolution, even in corrosive marine conditions. However, substantive coatings are absent on many particles allowing for more direct environmental reactivity with interior Fe-rich matrices;
- Fractures are more prevalent than reported in previous studies, with their size, number and configuration (linearity, connectivity) influenced by the dominant composition material. The largest fractures occurred in the particle with the highest relative Ca content;
- Many of the fractures connect pathways from the interior to the exterior surfaces indicating a potentially strong role in leaching radionuclides into the environment, but this has yet to be quantified;
- In all studied particles, the $^{239+240}$Pu activity concentrations are dominant, relative to ^{90}Sr and ^{137}Cs, which contrasts with particles from NPP accidents such as those from the Fukushima (^{137}Cs is dominant) and Chernobyl (both ^{90}Sr and ^{137}Cs are present). Compared with the NPP particles, the study particles have intense alpha and beta radioactivity (Pu isotopes) that raises long-term dose potentials if ingested or inhaled.

In future work, special focus is needed to link structural features more quantitatively with radioactivity leaching/dissolution rates associated with particles that may be inhaled/ingested, or when particles act as ongoing sources for radionuclide dispersal in the environment.

CRediT authorship contribution statement

M.P. Johansen: Conceptualization, Investigation, Data curation, Project administration, Writing. D.P. Child: Investigation, Formal analysis, Methodology, Writing. R. Collins: Investigation, Formal analysis; M. Cook: Writing, Validation. J. Davis: Formal analysis. M.A.C. Hotchkis; Formal analysis, Writing; D.L. Howard: Formal analysis, N. Howell; Formal analysis, Methodology. A. Ikeda-Ohno, Formal analysis, Methodology. E. Young: Investigation, Data curation, Writing.

Declaration of competing interest

The authors declare no competing interests.

Acknowledgements

We acknowledge the traditional owners of the lands addressed in this research as well as the government agencies that oversee resource and public protection programs and we hope this work is useful to them. Part of this research was undertaken on the XFM beamline at the Australian Synchrotron, part of ANSTO, Australia, which included expert advice from David Patterson and Martin de Jonge. Gamma and alpha analyses were performed by Lida Mokhber-Shahin, Sangeeth Thiruvoth and Jennifer Harrison. An important aspect of this study was the exposure of interior particle surfaces via polishing and this was expertly provided by Tim Palmer, ANSTO. Much thanks to Madison Hoffman, Edith Cowan University, for providing review comments. Advice on particle assessment methods was provided by members of the IAEA cooperative research project: Environmental Behaviour and Potential Biological Impact of Radioactive Particles (K41013). The IAEA is grateful to the Government of the Principality of Monaco for the support provided to its Environment Laboratories.

Appendix A. Supplementary data

Supplementary data to this article can be found online at https://doi.org/10.1016/j.scitotenv.2022.156755.

References

Abe, Y., Onozaki, S., Nakai, I., Adachi, K., Igarashi, Y., Oura, Y., et al., 2021. Widespread distribution of radiocesium-bearing microparticles over the greater Kanto region resulting from the Fukushima nuclear accident. Prog. Earth Planet. Sci. 8, 13.

ARL, 1986. Plutonium-contaminated fragments at the Taranaki site at Maralinga. In: Laboratory, A.R. (Ed.), Australian Radiation Laboratory, Melbourne, Australia.

ARL, 1990. Inhalation hazard assessment at Maralinga and Emu. ARL/TR087. Australian Radiation Laboratory, Melbourne, Australia.

Belloni, F., Himbert, J., Marzocchi, O., Romanello, V., 2011. Investigating incorporation and distribution of radionuclides in trinitite. J. Environ. Radioact. 102, 852–862.

Bellucci, J.J., Simonetti, A., 2012. Nuclear forensics: searching for nuclear device debris in trinitite-hosted inclusions. J. Radioanal. Nucl. Chem. 293, 313–319.

Bonamici, C.E., Kinman, W.S., Fournelle, J.H., Zimmer, M.M., Pollington, A.D., Rector, K.D., 2016. A geochemical approach to constraining the formation of glassy fallout debris from nuclear tests. Contrib. Mineral. Petrol. 172, 2.

Burakov, B.E., Shabalev, S.I., Anderson, E.B., 2003. Principal features of Chernobyl hot particles: phase, chemical and radionuclide compositions. In: Barany, S. (Ed.), Role of Interfaces in Environmental Protection. Springer, Netherlands, Dordrecht, pp. 145–151.

Burns, P.A., Cooper, M.B., Lokan, K.H., Wilks, M.J., Williams, G.A., 1995. Characteristics of plutonium and americium contamination at the former U.K. Atomic weapons test ranges at maralinga and emu. Appl. Radiat. Isot. 46, 1099–1107.

Caffrey, E.A., Johansen, M.P., Higley, K.A., 2015. Organ dose-rate calculations for small mammals at maralinga, the Nevada test site, Hanford and Fukushima: a comparison of ellipsoidal and voxelized dosimetric methodologies. Radiat. Res. 184, 433–441.

Caffrey, E.A., Johansen, M., Higley, K., 2017. Comparison of homogeneous and particulate lung dose rates for small mammals. Health Phys. 112 (6), 526–532. https://doi.org/10.1097/HP.0000000000000668.

Chen, Q., Peng, W., Yu, R., Tao, G., Nimbalkar, S., 2021. Laboratory investigation on particle breakage characteristics of calcareous sands. Adv. Civ. Eng. 2021, 8867741.

Child, D.P., Hotchkis, M.A.C., 2013. Plutonium and uranium contamination in soils from former nuclear weapon test sites in Australia. Nucl. Instrum. Methods Phys. Res., Sect. B 294, 642–646.

COMET, 2017. Final Report of the European Commission Funded COMET-RATE Project, Deliverable 3.4. Contract Number: Fission-2012-3.4.1-604794. European Commission.

Cook, M., Etschmann, B., Ram, R., Ignatyev, K., Gervinskas, G., Conradson, S.D., et al., 2021. The nature of Pu-bearing particles from the Maralinga nuclear testing site, Australia. Sci. Rep. 11, 10698.

Cooper, M., Burns, P., Tracy, B., Wilks, M., Williams, G., 1994. Characterization of plutonium contamination at the former nuclear weapons testing range, at maralinga in South Australia. J. Radioanal. Nucl. Chem. 177, 161–184.

Durbin, P.W., 1975. Plutonium in mammals: influence of plutonium chemistry, route of administration, and physiological status of the animal on initial distribution and long-term metabolism. Health Phys. 29, 495–510.

Eriksson, M., Lindahl, P., Roos, P., Dahlgaard, H., Holm, E., 2008. U, Pu, and Am nuclear signatures of the Thule hydrogen bomb debris. Environ. Sci. Technol. 42, 4717–4722.

Hancock, G.J., Leslie, C., Everett, S.E., Tims, S.G., Brunskill, G.J., Haese, R., 2011. Plutonium as a chronomarker in australian and New Zealand sediments: a comparison with (137)Cs. J. Environ. Radioact. 102, 919–929.

Harrison, J.J., Zawadzki, A., Chisari, R., Wong, H.K.Y., 2011. Separation and measurement of thorium, plutonium, americium, uranium and strontium in environmental matrices. J. Environ. Radioact. 102, 896–900.

Hotchkis, M.A.C., Child, D.P., Froehlich, M.B., Wallner, A., Wilcken, K., Williams, M., 2019. Actinides AMS on the VEGA accelerator. Nucl. Instrum. Methods Phys. Res., Sect. B 438, 70–76.

Howard, D.L., de Jonge, M.D., Afshar, N., Ryan, C.G., Kirkham, R., Reinhardt, J., et al., 2020. The XFM beamline at the Australian Synchrotron. J. Synchrotron Radiat. 27, 1447–1458.

IAEA, 2011. Radioactive Particles in the Environment: Sources, Particle Characterization and Analytical Techniques. IAEA-TECDOC-1663 IAEA, Vienna, Austria.

ICRP, 1986. The metabolism of plutonium and related elements. ICRP Publication 48; Vol 16. The International Commission on Radilolgical Protection.

Igarashi, J., Zheng, J., Zhang, Z., Ninomiya, K., Satou, Y., Fukuda, M., et al., 2019. First determination of pu isotopes (239Pu, 240Pu and 241Pu) in radioactive particles derived from Fukushima daiichi nuclear power plant accident. Sci. Rep. 9, 11807.

Ikeda-Ohno, A., Shahin, L.M., Howard, D.L., Collins, R.N., Payne, T.E., Johansen, M.P., 2016. Fate of plutonium at a former nuclear testing site in Australia. Environ. Sci. Technol. 50, 9098–9104.

Jernström, J., Eriksson, M., Simon, R., Tamborini, G., Bildstein, O., Marquez, R.C., et al., 2006. Characterization and source term assessments of radioactive particles from Marshall Islands using non-destructive analytical techniques. Spectrochim. Acta B At. Spectrosc. 61, 971–979.

Johansen, M.P., Child, D.P., Davis, E., Doering, C., Harrison, J.J., Hotchkis, M.A., et al., 2014. Plutonium in wildlife and soils at the maralinga legacy site: persistence over decadal time scales. J. Environ. Radioact. 131, 72–80.

Johansen, M.P., Child, D.P., Caffrey, E.A., Davis, E., Harrison, J.J., Hotchkis, M.A., et al., 2016. Accumulation of plutonium in mammalian wildlife tissues following dispersal by accidental-release tests. J. Environ. Radioact. 151 (Pt 2), 387–394.

Johansen, M.P., Child, D.P., Cresswell, T., Harrison, J.J., Hotchkis, M.A.C., Howell, N.R., et al., 2019. Plutonium and other radionuclides persist across marine-to-terrestrial ecotopes in the Montebello Islands sixty years after nuclear tests. Sci. Total Environ. 691, 572–583.

Johansen, M.P., Child, D.P., Hotchkis, M.A.C., Johansen, A., Thiruvoth, S., Whiting, S.D., 2020. Radionuclides in sea turtles at the Montebello Islands former nuclear test sites: current and historical dose rates for adults and embryos. Mar. Pollut. Bull. 158, 111390.

Johansen, M.P., Anderson, D., Child, D., Hotchkis, M.A.C., Tsukada, H., Okuda, K., et al., 2021. Differentiating Fukushima and Nagasaki plutonium from global fallout using 241Pu/239Pu atom ratios: Pu vs. Cs uptake and dose to biota. Sci. Total Environ. 754, 141890.

Kashparov, V., Salbu, B., Levchuk, S., Protsak, V., Maloshtan, I., Simonucci, C., et al., 2019. Environmental behaviour of radioactive particles from Chernobyl. J. Environ. Radioact. 208–209, 106025.

Kim, C.S., Lee, M.H., Kim, C.K., Kim, K.H., 1998. 90Sr, 137Cs, 239 + 240Pu and 238Pu concentrations in surface soils of Korea. J. Environ. Radioact. 40, 75–88.

Konzen, K., 2016. 241Am ingrowth and its effect on internal dose. Health Phys. 111, 22–29.

Kurihara, E., Takehara, M., Suetake, M., Ikehara, R., Komiya, T., Morooka, K., et al., 2020. Particulate plutonium released from the Fukushima daiichi meltdowns. Sci. Total Environ. 743, 140539.

Kuriny, V.D., Ivanov, Y.A., Kashparov, V.A., Loshchilov, N.A., Protsak, V.P., Yudin, E.B., et al., 1993. Particle-associated Chernobyl fall-out in the local and intermediate zones. Ann. Nucl. Energy 20, 415–420.

Lal, R., Fifield, L.K., Tims, S.G., Wasson, R.J., 2017. (239)Pu fallout across continental Australia: implications on (239)Pu use as a soil tracer. J. Environ. Radioact. 178–179, 394–403.

Lewis, L.A., Knight, K.B., Matzel, J.E., Prussin, S.G., Zimmer, M.M., Kinman, W.S., et al., 2015. Spatially-resolved analyses of aerodynamic fallout from a uranium-fueled nuclear test. J. Environ. Radioact. 148, 183–195.

Li, H.Y., Chai, H.W., Xiao, X.H., Huang, J.Y., Luo, S.N., 2020. Fractal breakage of porous carbonate sand particles: microstructures and mechanisms. Powder Technol. 363, 112–121.

Lind, O.C., Salbu, B., Janssens, K., Proost, K., García-León, M., García-Tenorio, R., 2007. Characterization of U/Pu particles originating from the nuclear weapon accidents at palomares, Spain, 1966 and thule, Greenland, 1968. Sci. Total Environ. 376, 294–305.

Lind, O.C., Tschiersch, J., Salbu, B., 2020. Nanometer-micrometer sized depleted uranium (DU) particles in the environment. J. Environ. Radioact. 211, 106077.

Long, S., Cook, M., C, F., J, C., 2021. Rehabilitation of the former nuclear test site at Maralinga. J. Radiol. Prot. 41, s46–s55.

Lukashenko, S., Kabdyrakova, A., Lind, O.C., Gorlachev, I., Kunduzbayeva, A., Kvochkina, T., et al., 2020. Radioactive particles released from different sources in the semipalatinsk test site. J. Environ. Radioact. 216, 106160.

MARTAC, 2003. Rehabilitation of the former nuclear test sites at Emu and Maralinga (Australia). Commonwealth of Australia, Canberra, Australia.

Martin, P.G., Jones, C.P., Cipiccia, S., Batey, D.J., Hallam, K.R., Satou, Y., et al., 2020. Compositional and structural analysis of Fukushima-derived particulates using high-resolution x-ray imaging and synchrotron characterisation techniques. Sci. Rep. 10, 1636.

Miura, H., Ishimaru, T., Ito, Y., Kurihara, Y., Otosaka, S., Sakaguchi, A., et al., 2021. First isolation and analysis of caesium-bearing microparticles from marine samples in the Pacific coastal area near Fukushima prefecture. Sci. Rep. 11, 5664.

Morooka, K., Kurihara, E., Takehara, M., Takami, R., Fueda, K., Horie, K., et al., 2021. New highly radioactive particles derived from Fukushima daiichi reactor unit 1: properties and environmental impacts. Sci. Total Environ. 773, 145639.

Muramatsu, Y., Rühm, W., Yoshida, S., Tagami, K., Uchida, S., Wirth, E., 2000. Concentrations of 239Pu and 240Pu and their isotopic ratios determined by ICP-MS in soils collected from the Chernobyl 30-km zone. Environ. Sci. & Technol. 34, 2913–2917.

Nakamura, S., Kajimoto, T., Tanaka, K., Yoshida, H., Maeda, M., Endo, S., 2018. Measurement of 90Sr radioactivity in cesium hot particles originating from the Fukushima nuclear power plant accident. J. Radiat. Res. 59, 677–684.

Papp, Z., Bolyos, A., Dezso, Z., Daroczy, S., 1997. Direct determination of 90Sr and 147Pm in Chernobyl hot particles collected in Kiev using Beta absorption method. Health Phys. 73, 944–952.

Pineau, A., Benzerga, A.A., Pardoen, T., 2016. Failure of metals I: brittle and ductile fracture. Acta Mater. 107, 424–483.
Pöllänen, R., Valkama, I., Toivonen, H., 1997. Transport of radioactive particles from the Chernobyl accident. Atmos. Environ. 31, 3575–3590.
Salbu, B., Lind, O.C., 2020. Analytical techniques for charactering radioactive particles deposited in the environment. J. Environ. Radioact. 211, 106078.
Salbu, B., Kashparov, V., Lind, O.C., Garcia-Tenorio, R., Johansen, M.P., Child, D.P., et al., 2018. Challenges associated with the behaviour of radioactive particles in the environment. J. Environ. Radioact. 186, 101–115.
Sancho, C., García-Tenorio, R., 2019. Radiological evaluation of the transuranic remaining contamination in palomares (Spain): a historical review. J. Environ. Radioact. 203, 55–70.
Satou, Y., Sueki, K., Sasa, K., Adachi, K., Igarashi, Y., 2016. First successful isolation of radioactive particles from soil near the Fukushima daiichi nuclear power plant. Anthropocene 14, 71–76.
Sheard, M., Lintern, M., Prescott, J., Huntley, D., 2006. Great Victoria Desert: new dates for South Australia's oldest desert dune system. Mesa J. 42, 15–26.
Smith, B.S., Child, D.P., Fierro, D., Harrison, J.J., Heijnis, H., Hotchkis, M.A.C., et al., 2016. Measurement of fallout radionuclides, 239,240Pu and 137Cs, in soil and creek sediment: Sydney Basin, Australia. J. Environ. Radioact. 151, 579–586.
Tims, S.G., Fifield, L.K., Hancock, G.J., Lal, R.R., Hoo, W.T., 2013. Plutonium isotope measurements from across continental Australia. Nucl. Inst. Methods Phys. Res. Sect. B Beam Interact. Mater. Atoms 294, 636–641.
UNSCEAR, 2000. United Nations Scientific Committee on the Effects of Atomic Radiation, UNSCEAR 2000 Report to the General Assembly, with Scientific Annexes. Annex C, Vienna.
Weisz, D.G., Jacobsen, B., Marks, N.E., Knight, K.B., Isselhardt, B.H., Matzel, J.E., et al., 2017. Deposition of vaporized species onto glassy fallout from a near-surface nuclear test. Geochim. Cosmochim. Acta 201, 410–426.
Wendel, C.C., Fifield, L.K., Oughton, D.H., Lind, O.C., Skipperud, L., Bartnicki, J., et al., 2013. Long-range tropospheric transport of uranium and plutonium weapons fallout from semipalatinsk nuclear test site to Norway. Environ. Int. 59, 92–102.
Whicker, F.W., Schultz, V., 1982. Radioecology: Nuclear Energy and the Environment. CRC Press, Boca Raton, Florida.
Yamaguchi, N., Mitome, M., Kotone, A.-H., Asano, M., Adachi, K., Kogure, T., 2016. Internal structure of cesium-bearing radioactive microparticles released from Fukushima nuclear power plant. Sci. Rep. 6, 20548.
Zheng, J., Tagami, K., Uchida, S., 2013. Release of plutonium isotopes into the environment from the Fukushima daiichi nuclear power plant accident: what is known and what needs to be known. Environ. Sci. Technol. 47, 9584–9595.